Intermetallics 91 (2017) 16–21

Contents lists available at ScienceDirect

Intermetallics

journal homepage: www.elsevier.com/locate/intermet

Martensitic transformation to monoclinic phase in bulk B2–CuZr

Nicolás Amigo[a,b,*], Matías Sepúlveda-Macías[a], Gonzalo Gutiérrez[a]

[a] Grupo de NanoMateriales, Departamento de Física, Facultad de Ciencias, Universidad de Chile, Casilla 653, Santiago, Chile
[b] Departamento de Ingeniería Mecánica, Facultad de Ciencias Físicas y Matemáticas, Universidad de Chile, Santiago, Chile

ARTICLE INFO

Keywords:
A. Shape–memory alloys
B. Martensitic transformation
C. Molecular dynamics simulation
D. Mechanical properties

ABSTRACT

Shape memory alloys, like B2–CuZr, are a class of materials that have the ability to recover their original shape when subjected to specific thermomechanical conditions. In this work, we carry out molecular dynamics simulations of bulk B2–CuZr to study its martensitic transformation at atomic level. For this purpose, uniaxial tensile tests are performed at temperatures ranging from 1 K to 600 K. We show that all cases exhibit pseudoelasticity by undergoing phase transition from B2 to monoclinic phase along the {110} planes, instead to an R phase as reported in previous works. We obtain the Bain path employing two different interatomic potentials. One potential exhibits martensitic transformation from B2 to monoclinic to body–centered tetragonal structure, while using the other potential a transition from B2 to monoclinic structure is observed, being absent the body–centered tetragonal phase. Reversibility of this transformation is confirmed by performing uniaxial tensile/compressive tests. Finally, a stress–temperature phase diagram is presented as a tool to estimate the stress required to initiate martensitic transformation of bulk B2–CuZr phases.

1. Introduction

Martensitic transformation (MT) is a mechanism which appears in different engineering functional materials, such as strengthened steel, polymers and shape memory alloys (SMAs). An outstanding property of MT is its reversibility to go from one phase to another under certain thermomechanical or magnetic conditions. Thus, SMAs have been employed in many engineering fields, such as structures and composites [1], automotive [2], aerospace [3] and micro-electromechanical systems (MEMS) [4]. Among the different SMAs available in the industry, of our interest is the case of the B2–CuZr alloy due to its application in metallic glasses (MG). It is widely known that MGs posses high yield strength and hardness, but suffer from poor ductility and brittle fracture, which limit their applications. To overcome this difficulty, it has been proposed to manufacture shape memory metallic glass composites. The main concept is to integrate a SMA as a crystalline phase in bulk MG to produce transformation induced plasticity [5,6]. In the case of CuZr–based MGs, experimental results have reported that mechanical properties are enhanced when high volume fractions of the B2 crystalline phase, for instance 40–80%, are found in the system. It has also been observed that the stress–strain curve of the MG exhibits more than one yield point due to the MT and that plastic flow is stabilized with high concentrations of the crystalline phase, improving the ductility of the MG [7–9]. Regarding theoretical studies, it is important to remark that there exists a lack of works about the B2–CuZr system at the atomic level to further discuss this MT, since most of the available literature concentrates solely in the structural and mechanical properties of CuZr MGs [10–14] without the presence of any crystalline phase.

Molecular dynamics (MD) simulations have been performed in recent years to study the B2–CuZr system and its MT in order to give an atomic level description. Sutrakar et al. [15,16] carried out tensile tests of B2–CuZr nanowires. He reported that these nanowires exhibited a MT from an initial B2 phase to a final BCT phase via nucleation and propagation of {100} planes, where an intermediate R phase was observed. These findings were also supported by Cheng et al. [17] and Sopu et al. [18]. In addition, Cheng et al. stated that the BCT phase was a metastable one, which was later discussed by Sutrakar et al. [19], concluding that this phase is unstable. However, none of these authors observed a B2 to monoclinic transformation, which has been largely reported in experimental results [7,9,20]. Moreover, these authors employed only the first version of the interatomic potential for the CuZr alloy developed by Mendelev et al. [21], which overestimates the Cu–Zr interaction. This drawback, among others, was overcome in a new version of the CuZr potential [22], where new data from experimental and first principles calculations were introduced to improve the accuracy of the semi–empirical potential. Thus, it is important to revisit the phase transformation of B2–CuZr samples using both potentials.

Thus, in order to get a better insight of B2–CuZr phase transformation, at an atomic level, some fundamental questions about its martensitic transformation should be addressed, for instance, what are

* Corresponding author. Departamento de Ingeniería Mecánica, Facultad de Ciencias Físicas y Matemáticas, Universidad de Chile, Santiago, Chile.
E-mail addresses: nico.amigo.a@gmail.com (N. Amigo), msepmacias@gmail.com (M. Sepúlveda-Macías), gonzalogutierrez@uchile.cl (G. Gutiérrez).

http://dx.doi.org/10.1016/j.intermet.2017.08.003
Received 1 July 2017; Received in revised form 27 July 2017; Accepted 2 August 2017
Available online 09 August 2017

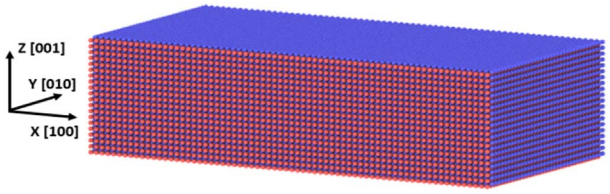

Fig. 1. Bulk B2–CuZr with periodic boundary conditions.

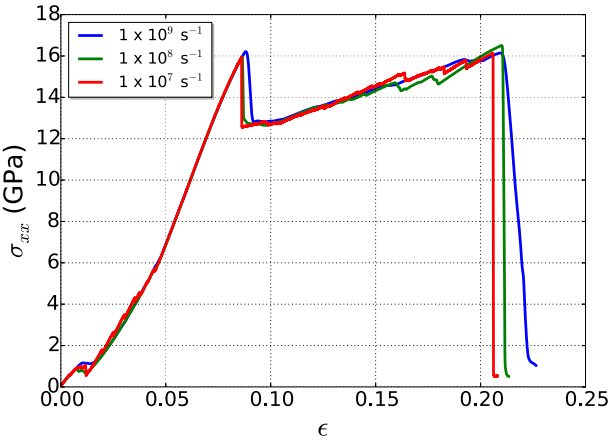

Fig. 2. Uniaxial tensile test of bulk B2–CuZr at 1 K and different strain rates.

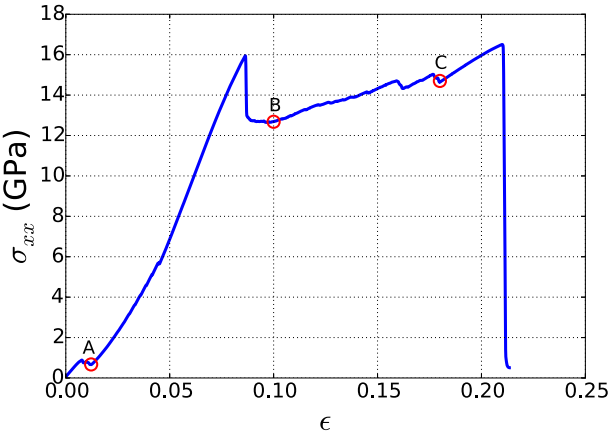

Fig. 3. Stress–strain curve for bulk B2–CuZr at 1 K and at 10^8 s^{-1} strain rate.

the structures of B2–CuZr along the transformation?, is the final structure stable?, what are the transformation paths? and finally, under what thermomechanical parameters the transformation takes place? The main goal of this work is to provide an answer to these questions.

In this work, we carry out MD simulations of bulk B2–CuZr under uniaxial tensile loading considering different temperatures, ranging from 1 K to 600 K, as well as different strain rates. Bulk systems have been selected over nanowires in order to neglect surface effects and to ease structural and phase transformation analysis. Also, the Bain path is calculated using both interatomic potentials developed by Mendelev et al. [21,22], in order to elucidate the differences in the MT. Reversibility of the transformation is checked and a stress–temperature phase diagram is obtained. This paper is organized as follows: in Section 2 we explain the simulation procedure and the tools for analysis used, in section 3 we present and discuss our results, and in Section 4 we draw the conclusions.

2. Simulation details

The B2–CuZr system under study has dimensions of 226.8 × 113.4 × 64.8 Å^3, with a lattice parameter of 3.24 Å and containing 98000 atoms, as shown in Fig. 1, where Cu and Zr atoms are colored blue and red, respectively. Periodic boundary conditions are imposed in all directions. To perform molecular dynamics simulations, it is necessary to adopt an adequate interatomic potential. In this work we employ the embedded-atom method (EAM) potential proposed by Mendelev et al. [22] for the CuZr system. The EAM gives the total energy of an atomic system in the form

$$E_i = F_\alpha\left(\sum_{j\neq i}\rho_\beta(r_{ij})\right) + \frac{1}{2}\sum_{j\neq i}\varphi_{\alpha\beta}(r_{ij}), \tag{1}$$

where F is the embedding energy which is a function of the atomic electron density ρ. In the second term, φ is a pair potential interaction and α and β are the element types of atoms i and j.

In order to carry out uniaxial tensile tests in bulk B2–CuZr, the molecular dynamics code LAMMPS developed by Plimpton et al. [23] is used. The procedure of the simulations is the following. Firstly, the energy of the system is minimized using the conjugate gradient method. Secondly, the Langevin thermostat at a constant temperature T and the Berendsen barostat at zero pressure are applied for 100 ps, using 1 fs as the integration time step. T is the target temperature to be studied, ranging from 1 K to 600 K. After these two steps, the sample is loaded along the [100] direction. Three different strain rates are considered, namely, 10^7 s^{-1}, 10^8 s^{-1} and 10^9 s^{-1}. The strain is applied on the system by rescaling the positions of atoms each time step. The temperature is kept constant at T using the Langevin thermostat. In order to analyze our simulation, we use several diagnostic tools. For stress–strain curve, we evaluate the σ_{xx} component of the stress tensor, as well as the axial component of the strain tensor, denoted as ε. The analysis of the atomic structure is made by means of the pair distribution function, the common neighbor analysis (CNA) [24,25] and the local atomic shear strain η^{Mises} [26]. This parameter requires two atomic configurations, the current and the reference one. The first step is to seek a local affine transformation $\mathbf{J}_i$ that best map

$$\{\mathbf{d}^0_{ji}\} \rightarrow \{\mathbf{d}_{ji}\},\ \forall\, j \in N^0_i, \tag{2}$$

where $\mathbf{d}$ are vector separations between atom i and each neighbor j. Here the superscript 0 stands for reference configuration, and N^0_i is the number of neighbors of atom i at the reference configuration. Then, we seek $\mathbf{J}_i$ that minimizes

$$\sum_{j\in N^0_i}\left|\mathbf{d}^0_{ji}\mathbf{J}_i - \mathbf{d}_{ji}\right|^2 \rightarrow \mathbf{J}_i = \left(\sum_{j\in N^0_i}\mathbf{d}^{0T}_{ji}\mathbf{d}^0_{ji}\right)^{-1}\left(\sum_{j\in N^0_i}\mathbf{d}^{0T}_{ji}\mathbf{d}_{ji}\right). \tag{3}$$

With $\mathbf{J}_i$, the Lagrangian strain matrix can be calculated as

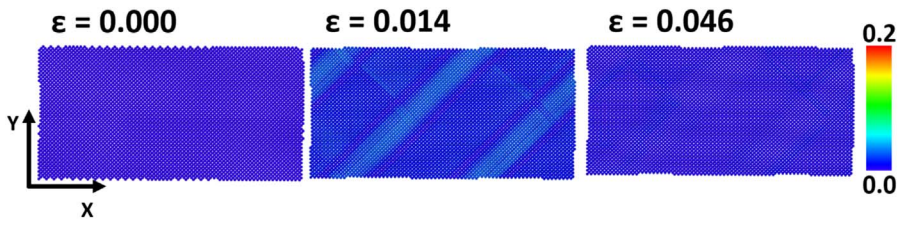

Fig. 4. Bulk B2–CuZr at different strains. Atoms are colored according to the local atomic shear strain. (For interpretation of the references to colour in this figure legend, the reader is referred to the web version of this article.)

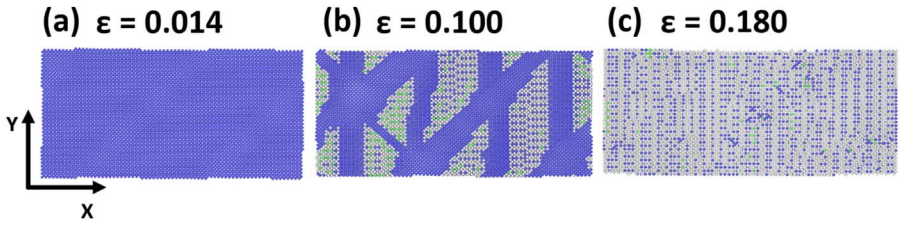

Fig. 5. CNA performed in stages (a) A, (b) B and (c) C marked in Fig. 3. Blue atoms have B2 structure and grey atoms have M structure. (For interpretation of the references to colour in this figure legend, the reader is referred to the web version of this article.)

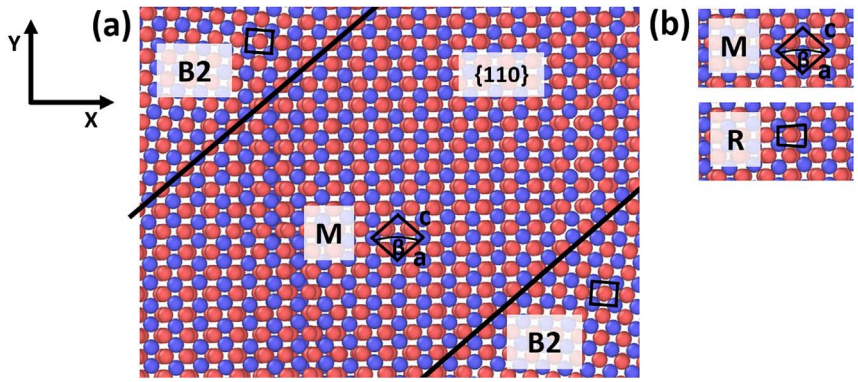

Fig. 6. (a) A phase transformation band in a {110} plane at ε = 0.16. (b) Comparison between the M phase defined in this work and the R phase defined by Sutrakar et al. [16].

Table 1
Lattice parameters for the M phase.

Work	a (Å)	b (Å)	c (Å)	β (°)
Zhalko-titarenko et al. [30]	5.10	2.64	5.23	100.3
Uporov et al. [31]	5.09	2.66	5.23	100.5
Tensile test (this work)	4.98	2.73	5.10	100.8
Bain path M2007 (this work)	4.98	2.72	5.01	97.2
Bain path M2009 (this work)	4.98	2.70	5.03	98.6

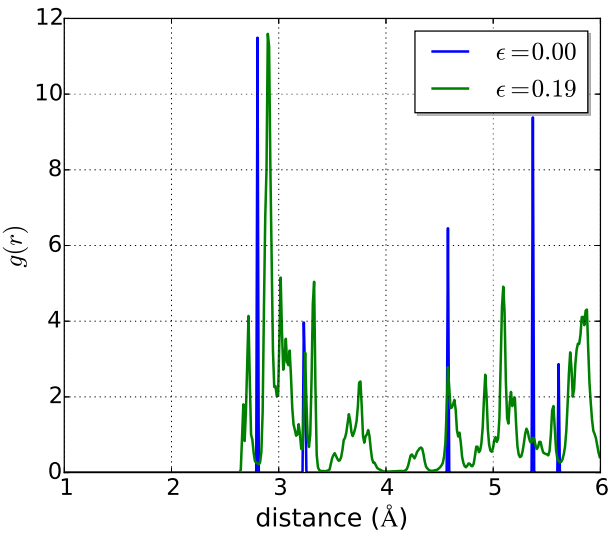

Fig. 7. Total pair distribution function of the system at (a) ε = 0.00 and (b) ε = 0.19.

$$\eta_i = \frac{1}{2}(\mathbf{J}_i\mathbf{J}_i^T - \mathbf{I}), \tag{4}$$

where the local shear invariant for atom i is defined as

$$\eta_i^{\text{Mises}} = \sqrt{\eta_{yz}^2 + \eta_{xz}^2 + \eta_{xy}^2 + \frac{(\eta_{yy} - \eta_{zz})^2 + (\eta_{xx} - \eta_{zz})^2 + (\eta_{xx} - \eta_{yy})^2}{6}}, \tag{5}$$

where $\eta_{\alpha\beta}$ are the components of the strain tensor of atom i. We visualize η_i^{Mises} using the software OVITO [27].

3. Results and discussion

3.1. Strain rate effect

The mechanical response of the bulk B2–CuZr system to different strain rates is explored by performing three uniaxial tensile tests, 10^7 s^{-1}, 10^8 s^{-1} and 10^9 s^{-1}. To avoid temperature effects, the system is kept at 1 K. The results are presented in Fig. 2. It is interesting to note that the three curves follow the general trend of MT, as will be discussed in the next Subsection. In this case, it is observed an elastic regime up to around 0.09. Then, the stress decays abruptly and a second elastic regime emerges, which is identified as pseudoelasticity. Finally, the three systems undergo fracture at ∼0.21. It is observed that the elastic limit at $\varepsilon \sim 0.09$ increases with the strain rate, which has been already discussed in the literature. The explanation is as follows: as the strain rate increases, atoms have less time to react mechanically, i.e. to initiate dislocation activity and MT, among others, which is known as phonon drag [28,29]. Beyond the elastic limit, the three cases undergo MT. It is also observed that the case at 10^9 s^{-1} exhibits a smooth curve, while the others two exhibit a sawtooth behavior due to phonon drag. The onset of fracture occurs at $\varepsilon \sim 0.21$. In the following, we perform tensile tests considering a strain rate of 10^8 s^{-1}, since it has no significant differences compared to the 10^7 s^{-1} strain rate and also has a lower computational cost.

3.2. Structural characterization of bulk B2–CuZr under tensile test

In order to give an atomic level structural characterization of the bulk B2–CuZr under tensile test at 10^8 s^{-1} and at 1 K, we focus our attention on three stages of the stress–strain curve labeled as A, B and C, which are shown in Fig. 3. These stages belong to three different atomic structure configurations, namely a pure B2, a combined B2 and M, and M. Here M denotes an atomic structure that we identify as monoclinic. Thus, according to the strain increases, MT takes place, from B2 to M. At stage A, that is $\varepsilon = 0.014$, the stress sightly decreases. The atomic level picture of this loss of stress is presented in Fig. 4, where atoms are colored according to the local atomic shear strain. It is observed that as the strain increases, there is a slight movement of atomic planes. Nevertheless, these planes go back to their original positions when the

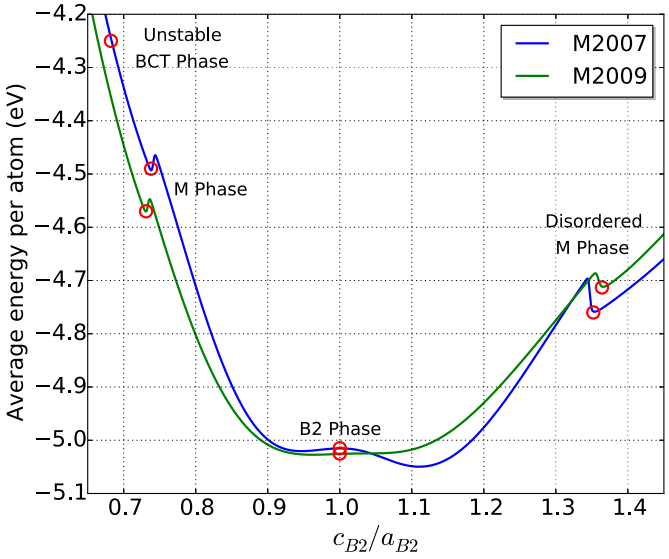

Fig. 8. Bain path of bulk B2–CuZr.

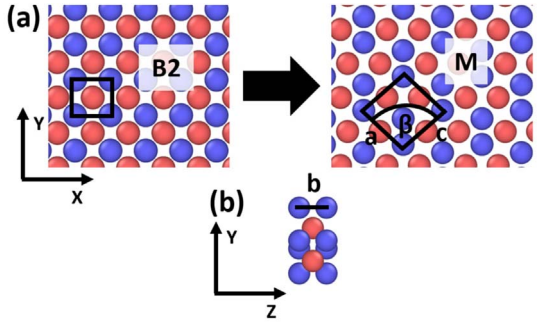

Fig. 9. (a) B2 to M transformation for case M2009. (b) Side view of the M structure.

stress drops, recovering the system its initial structure, as shown in Fig. 4 at $\varepsilon = 0.046$. A CNA analysis confirms that the entire system has a B2 structure (see Fig. 5 (a)).

At ε= 0.09, the system reaches its elastic limit and then a family of {110} planes appear. These planes form bands, which have atomic structure different than B2. To distinguish atoms with a B2 structure type with those of a different structure, CNA is performed and the results are presented in Fig. 5, where blue, green and white atoms represent B2, fcc and M crystal structures, respectively. Fig. 5 (b), i.e. stage B, shows phase transformation bands composed by atoms with fcc and M crystal structures. At higher strains these bands coalesce, as seen in Fig. 5 (c), which corresponds to stage C. Atoms of fcc structure appear for a few steps of simulation and then quickly become atoms of M structure.

To inspect the crystal structure of the bands, Fig. 6 (a) shows a region of the system at $\varepsilon = 0.16$. A thorough analysis reveals that the bands contain small clusters of M crystal structures. However, these structures are not uniform inside the bands and thus, no full transformation from B2 to M structure is observed. The three lattice parameters are calculated for some clusters, obtaining $a \sim 4.98$ Å, $c \sim 5.10$ Å as the length of the edges and $b \sim 2.73$ Å as the length of the height, with $\beta \sim 100.8°$, which are close to the M structure presented in previous experimental results [30,31]. Table 1 summarize these values. This M phase is shown in Fig. 6 (b) (top panel). The two structures displayed in Fig. 6 (b) are exactly the same, where the top panel corresponds with our identification (M phase) and the bottom panel corresponds to the identification as R phase given by other authors [15–18]. Thus, this phase transformation should be called a MT from B2 to M rather than from B2 to R phase. Pair distribution function is employed to compare the crystal structure of the system at $\varepsilon = 0.00$ with the one of the system at $\varepsilon = 0.19$, i.e. when all bands have coalesced. The result is observed in Fig. 7. At $\varepsilon = 0.00$, there are five peaks which define the B2 structure. On the other hand, at $\varepsilon = 0.19$, the main peak at $\sim$2.8 Å is displaced by $\sim$0.1 Å and the others are smoothed suggesting the absence of a dominant crystal structure in the bands. Nevertheless, a new peak has appeared at $\sim$5.1 Å which can be correlated to the lattice parameter c of the clusters of M phase.

3.3. Bain path of the transition from B2 to M in bulk B2–CuZr

To elucidate the mechanism of MT from B2 to M, molecular statics (MS) simulations are performed to calculate the Bain path. Two different interatomic potentials are used for CuZr: Mendelev et al. [21,22], which we call M2007 and M2009 hereafter, respectively. A sample of 5488 atoms, with periodic boundary conditions is considered. Tensile strain is applied along the [100] direction and simultaneously a compressive strain along the [010] and [001] directions. Also, a compressive strain is applied along the [100] direction and simultaneously a tensile strain along the [010] and [001] directions. We remark here that it is necessary to strain all directions at the same time in order to observe a phase transition from B2 to M, otherwise, the system fractures without any MT. After each simulation step, an energy minimization is performed and the average energy per atom is calculated, obtaining the energy curves shown in Fig. 8, where a_{B2} and c_{B2} are the lattice parameters of the B2 structure. For both M2009 and M2007 is observed that the system has a B2 phase at $c_{B2}/a_{B2} = 1$. As c_{B2}/a_{B2} decreases, the sample reaches a local minimum at $c_{B2}/a_{B2} = 0.73$, where the B2 structure transforms into a M structure, which is shown in Fig. 9 (a) and (b). This is the same M structure already found in the phase transformation bands described in Subsection 3.2, but now they are populating the whole system. Hence, we suggest that the tensile test performed above cannot provide the necessary stress to fully transform the system from a B2 phase to a M phase, since tensile strain along one direction and compressive strain along the others two are required. For the M2009 interatomic potential, the lattice parameters of the M phase are calculated as $a = 4.98$ Å, $b = 2.70$ Å and $c = 5.03$ Å, with β= 98.6° (see Fig. 9), which are in good agreement with those obtained in previous experimental results [30,31]. For the case M2007, see Table 1. It is interesting to note that in the case of M2007, further decreasing of c_{B2}/a_{B2} causes the sample to fully transform into an unstable body–centered tetragonal (BCT) structure (see Fig. 10). The use of this potential explains that other authors [15–18] had found transformation from B2 to M to BCT, which is absent in M2009. On the other hand, when c_{B2}/a_{B2} increases, the system reaches another local minimum at $c_{B2}/a_{B2} = 1.36$ for both potentials. Here, the system exhibits some clusters of M phase, but it is highly disordered, as shown in Fig. 11 for case M2009. Note that M2007 exhibits also a local minimum at

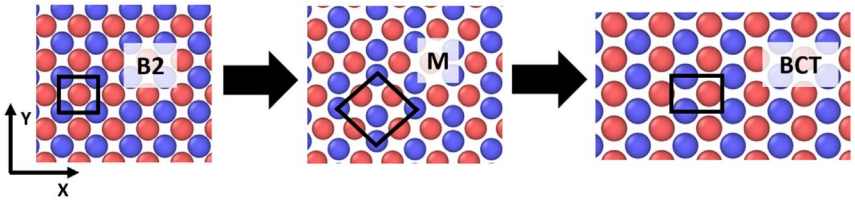

Fig. 10. B2 to M to BCT transformation for case M2007.

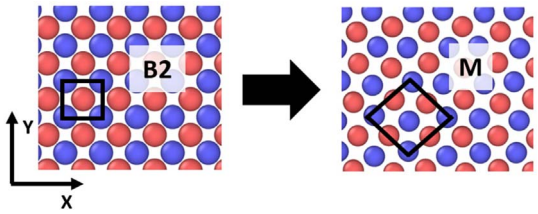

Fig. 11. B2 to disordered M phase transformation for case 2009.

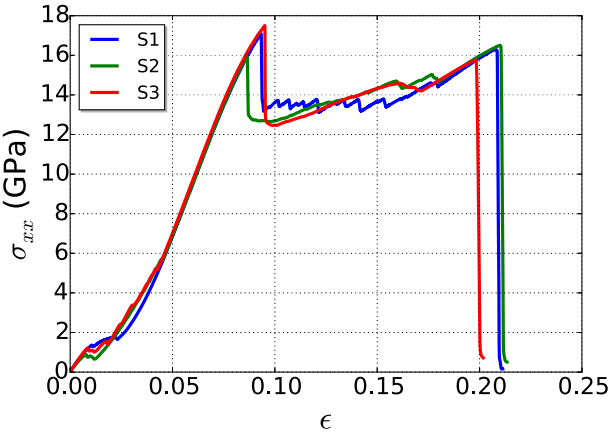

Fig. 12. Uniaxial tensile tests for bulk B2–CuZr systems of different size.

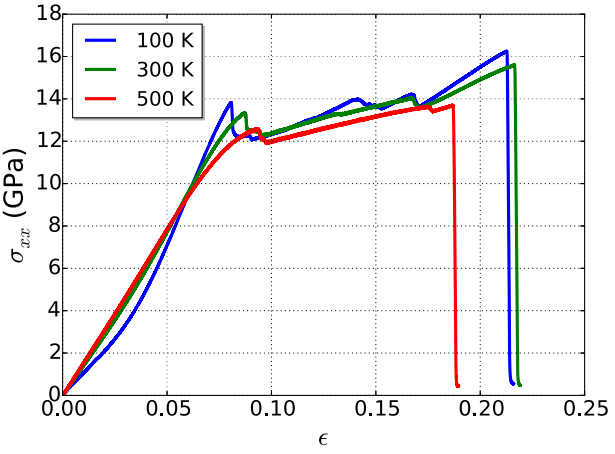

Fig. 13. Uniaxial tensile tests at different temperatures.

$c_{B2}/a_{B2} = 1.12$, but no MT is observed.

3.4. Size effect

Two more bulk B2–CuZr systems are considered to study the size effect on the martensitic transformation. Their dimensions are 226.80 × 55.1 × 32.40 Å^3 containing 23800 atoms and 226.8 × 226.8 × 129.6 Å^3 containing 392000 atoms, which we call sample 1 (S1) and sample 3 (S3), respectively. The system analyzed in Section 3.2 is called sample 2 (S2), since it is bigger than S1 but smaller than S3. Tensile tests are performed at 1 K and the results are shown in Fig. 12. The three cases exhibit a similar elastic regime and martensitic transformation. However, S1 exhibits a clear sawtooth behavior during its phase transformation, opposed to S2 and S3, which have a smoother transition as expected due to its higher number of atoms. Thus, qualitatively, the three samples present martensitic transformation and no relevant size effects are observed.

3.5. Temperature effect

Uniaxial tensile test at a constant temperature of 1 K allowed us to understand the crystal structure behavior of the sample avoiding temperature effects. In this section we proceed to include this effect by performing tensile tests at different constant temperatures, namely, 100, 300 and 500 K. The results are presented in Fig. 13. The most remarkable feature is that the decrease of stress at $\varepsilon = 0.01$ is no longer observed. Instead, the curve at 100 K exhibits an elastic regime, which can be considered as composed by two linear parts, one up to $\varepsilon = 0.03$ and another from 0.03 to 0.07 of strain, while the other two curves display a single linear elastic regime. The absence of the abrupt decrease of stress can be explained by considering the random motion of atoms due to the thermal effects. Since atoms move around their equilibrium sites, they adjust their positions slightly as the strain is applied, dampening the movement of planes commented in Subsection 3.2. At temperatures above 100 K, these movement disappears and a complete linear elastic regime is achieved. Hence, the sample can show a sawtooth–like elastic behavior (see Fig. 3), an elastic regime composed by two linear parts or a single linear elastic regime. On the other hand, the yield stress decreases as the temperature increases, as well as the stress required to fracture the system, which is in good agreement with previous studies [16]. In addition, all the systems exhibit phase transition from B2 to disordered M phase along the {110} planes, as was discussed in Subsection 3.2 for the case at 1 K. Overall, the temperature has the role to decrease the stress necessary to initiate the second elastic regime in the system.

3.6. Reversibility of martensitic transformation in bulk B2–CuZr

As it has been seen, MT occurs in the system when subjected to tensile test. However, it is relevant to confirm whether it is a reversible transformation or not. To shed light to this point, we perform tension and compression tests on samples at 1 K and 300 K. The results are presented in Fig. 14 (a) and (b) respectively. In both cases, there is an elastic regime up to $\varepsilon \sim 0.08$. Then, the samples undergo MT up to $\varepsilon \sim 0.15$, giving rise to a second elastic regime. Hence, pseudoelasticity is present in both curves. Then, at this strain the systems are compressed and fully recover their initial B2 structure. Hysteresis is observed during the process. It is interesting to note that when tension is applied, the sample at 1 K has to overcome a higher yield stress to initiate its second elastic regime, compared to the other case. Nevertheless, during compression, both cases go back to their first elastic regime at ~12 GPa. Hence, the energy dissipation is higher for the system at 1 K. These values are presented in Table 2. Since bulk B2–CuZr systems undergo reversible phase transformation, it is plausible to build a stress–temperature phase diagram in order to know the required stress and temperature to initiate the B2 to M transformation. For this purpose, we perform a set of uniaxial tensile tests. Each test is at a different constant temperature and their corresponding yield and fracture stresses are calculated. Using these values, the stress–temperature phase diagram is built, which is shown in Fig. 15. As it is seen, at higher temperatures, the stress required to initiate MT decreases. On the other hand, this trend is not completely observed to determine the onset of fracture. The precision of this phase diagram can be improved by considering several tensile tests at the same temperature and averaging the resulting yield and fracture stresses. Nevertheless, this diagram can be a useful tool for predicting phase transformation of B2–CuZr structures when subject to uniaxial tensile tests.

4. Conclusions

Molecular dynamics simulations have been performed to study the martensitic transformation of bulk B2–CuZr under uniaxial tensile tests. A temperature range from 1 K to 600 K was considered and an atomic level structural characterization was performed.

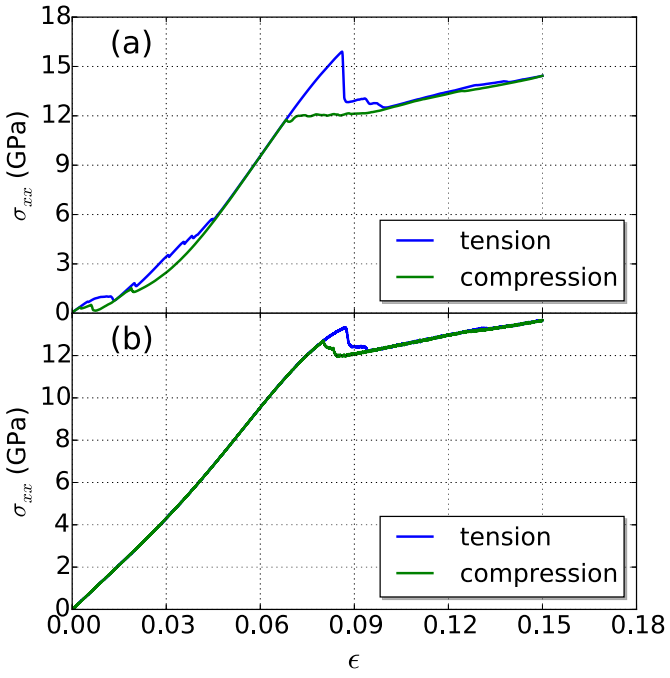

Fig. 14. Tensile and compressive tests for samples at (a) 1 K and (b) at 300 K.

Table 2
Energy dissipation for the tension and compression of the systems at 1 K and 300 K.

Temperature (K)	Energy dissipation (MJ/m^3)
1	74.0
300	9.6

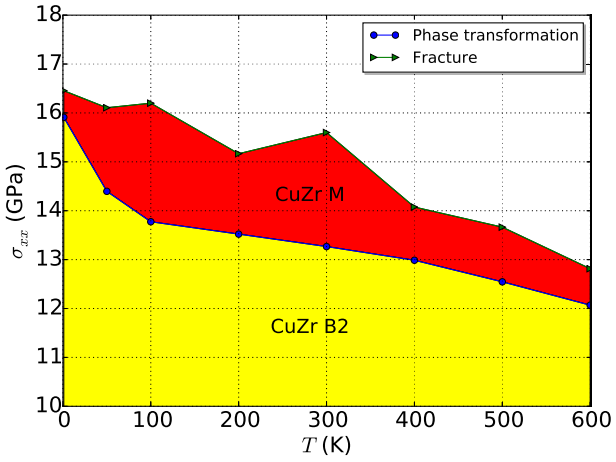

Fig. 15. $\sigma_{xx} - T$ phase diagram.

During the tensile tests, three regimes were identified. Firstly, the samples exhibited an elastic regime of pure B2 phase. Secondly, phase transition from B2 to monoclinic phase took place along the {110} planes. Lastly, a second elastic regime, corresponding to the monoclinic phase, was observed. Therefore, bulk B2–CuZr presents pseudoelasticity, transforming from its initial B2 phase to a final monoclinic structure, instead of an R phase as previously described by other authors [15–18].

The Bain path of bulk B2–CuZr was calculated using two different interatomic potentials, which we called M2007 [21] and M2009 [22]. For the former, the system underwent a two step phase transition, this is, from B2 to monoclinic to a final unstable body–centered tetragonal structure, which is in agreement with previous results of tensile tests [15–18]. Nevertheless, the M2009 interatomic potential only showed the B2 to monoclinic phase transition, which explains the absence of body–centered tetragonal phase during the tensile tests of this work.

Tension/compression tensile tests were carried out and it was observed that all samples exhibited reversibility. Hence, a stress–temperature phase diagram was constructed to predict the onset of martensitic transformation of bulk B2–CuZr at different temperatures.

All in all, we have shown by means of molecular dynamics, that bulk B2–CuZr is a shape memory alloy that undergoes phase transformation from an initial B2 structure to a final monoclinic phase, which makes the B2–CuZr system a suitable alloy to enhance ductility of metallic glasses. In addition, the stress–temperature phase diagram presented in this work can be employed as a diagnostic tool to estimate the required stress to initiate martensitic transformation of B2–CuZr precipitates in metallic glasses under tensile tests.

Acknowledgments

N.A. thanks to CONICyT PhD fellowship No. 21151448, M.S-M. thanks to CONICyT Ph.D. fellowship No. 21140904 and G.G thanks to grant PAIFAC 2016, Facultad de Ciencias, Universidad de Chile.

References

[1] Y. Furuya, J. Intell. Mater. Syst. Struct. 7 (1996) 321–330.
[2] D. Stoeckel, Mater. Des. 11 (1990) 302–307.
[3] D.J. Hartl, D.C. Lagoudas, Proc. Inst. Mech. Eng. Part G J. Aerosp. Eng. 221 (2007) 535–552.
[4] L. Sun, W. Huang, Z. Ding, Y. Zhao, C. Wang, H. Purnawali, C. Tang, Mater. Des. 33 (2012) 577–640.
[5] D.C. Hofmann, Science 329 (2010) 1294–1295.
[6] S. Pauly, S. Gorantla, G. Wang, U. Kuhn, J. Eckert, Nat. Mater. 9 (2010) 473–477.
[7] K. Song, S. Pauly, Y. Zhang, R. Li, S. Gorantla, N. Narayanan, U. Khn, T. Gemming, J. Eckert, Acta Mater. 60 (2012) 6000–6012.
[8] K.K. Song, S. Pauly, B.A. Sun, J. Tan, M. Stoica, U. Kuhn, J. Eckert, AIP Adv. 3 (2013) 012116.
[9] F. Wu, K. Chan, S. Chen, S. Jiang, G. Wang, Mater. Sci. Eng. A 636 (2015) 502–506.
[10] J. Wachter, G. Gutiérrez, A. Zuñiga, R. Palma, J. Mater. Sci. 49 (2014) 8051–8056.
[11] C. Tang, C. Wong, Intermetallics 58 (2015) 50–55.
[12] M. Sepúlveda-Macías, N. Amigo, G. Gutiérrez, J. Alloy. Compd. 655 (2016) 357–363.
[13] Y. Ye, S. Wang, J. Fan, C. Liu, Y. Yang, Intermetallics 68 (2016) 5–10.
[14] M. Celtek, S. Sengul, U. Domekeli, Intermetallics 84 (2017) 62–73.
[15] V.K. Sutrakar, D.R. Mahapatra, Mater. Lett. 63 (2009) 1289–1292.
[16] V.K. Sutrakar, D.R. Mahapatra, Intermetallics 18 (2010) 679–687.
[17] Y.Q. Cheng, E. Ma, H.W. Sheng, Phys. Rev. Lett. 102 (2009) 245501.
[18] D. Sopu, M. Stoica, J. Eckert, Appl. Phys. Lett. 106 (2015) 211902.
[19] V.K. Sutrakar, D.R. Mahapatra, Appl. Phys. Lett. 95 (2009) 136101.
[20] Y. Koval, G. Firstov, A. Kotko, Scr. Metallurgica Mater. 27 (1992) 1611–1616.
[21] M.I. Mendelev, D.J. Sordelet, M.J. Kramer, J. Appl. Phys. 102 (2007) 1–7.
[22] M.I. Mendelev, M.J. Kramer, R.T. Ott, D.J. Sordelet, D. Yagodin, P. Popel, Philos. Mag. 89 (2009) 967–987.
[23] S. Plimpton, J. Comput. Phys. 117 (1995) 1–19.
[24] J.D. Honeycutt, H.C. Andersen, J. Phys. Chem. 91 (1987) 4950–4963.
[25] A. Stukowski, Model. Simul. Mater. Sci. Eng. 20 (2012) 045021.
[26] F. Shimizu, S. Ogata, J. Li, Mater. Trans. 48 (2007) 2923–2927.
[27] A. Stukowski, Model. Simul. Mater. Sci. Eng. 18 (2010) 015012.
[28] M.F. Horstemeyer, M.I. Baskes, S.J. Plimpton, Acta Mater. 49 (2001) 4363–4374.
[29] W. Liang, M. Zhou, Proc. Inst. Mech. Eng. Part C J. Mech. Eng. Sci. 218 (2004) 599–606.
[30] A.V. Zhalko-Titarenko, M.L. Yevlashina, V.N. Antonov, B.Y. Yavorskii, Y.N. Koval, G.S. Firstov, Phys. Status Solidi (b) 184 (1994) 121–127.
[31] S.A. Uporov, S.K. Estemirova, N.M. Chtchelkatchev, R.E. Ryltsev, J. Alloy. Compd. 647 (2015) 397–401.